J Mater Sci (2014) 49:7648–7658
DOI 10.1007/s10853-014-8473-z

Application of Ni and Cu nanoparticles in transient liquid phase (TLP) bonding of Ti-6Al-4V and Mg-AZ31 alloys

Anas M. Atieh · Tahir I. Khan

Received: 27 May 2014 / Accepted: 14 July 2014 / Published online: 30 July 2014

Abstract The transient liquid phase (TLP) bonding of Ti-6Al-4V alloy to a Mg-AZ31 alloy was performed using an electrodeposited Ni coating containing a dispersion of Ni and Cu nanoparticles. Bond formation was attributed to two mechanisms; first, solid-state diffusion of Ni and Mg, followed by liquid eutectic formation at the Mg-AZ31 interface. Second, the solid-state diffusion of Ni and Ti at the Ti-6Al-4V interface resulted in a metallurgical joint. The joint interface was characterized by scanning electron microscopy, energy dispersive X-ray spectroscopy, and X-ray diffraction analysis. Microhardness and shear strength tests were used to investigate the mechanical properties of the bonds. The use of Cu nanoparticles as a dispersion produced the maximum joint shear strength of 69 MPa. This shear strength value corresponded to a 15 % enhancement in joint strength compared to TLP bonds made without the use of nanoparticles dispersion.

Introduction

In recent years, there has been an increase in the demand on advanced structural and engineering applications requiring the use of joining techniques with the capabilities of bonding dissimilar alloys [1–3]. Transient liquid phase (TLP) diffusion bonding is a joining technique that is been used as an alternative to join dissimilar alloys which cannot be joined by conventional welding techniques such as fusion welding [2, 4, 5]. The TLP diffusion bonding parameters include bonding time, pressure, temperature, and interlayer characteristics (e.g., coating or foil). In recent studies, Ni foils have been used to produce joints between Mg-AZ31 and Ti-6Al-4V alloys with satisfactory joint strength (39 MPa) [6]. However, further enhancement in joint strength was achieved by a Ni/Cu double sandwich foil configuration (57 MPa) [7]. Furthermore, the use of thin Ni electrodeposited coats resulted in better joint quality and strength (61 MPa), when compared with joints made with Ni foils [6, 7]. Therefore, the literature shows that the quality of bonds produced by TLP bonding is significantly affected by the interlayer characteristics which affect microstructural development across the bond region and the subsequent joint strengths [8–13]. Furthermore, in recent work, it has been shown that the presence of a nanoparticle dispersion in a coating (i.e. Ni/Al_2O_3) can also be used as a method of strengthening the joint region [13–15].

Ti-6Al-4V alloy is an α–β titanium alloy, and has been used in a number of engineering applications including aerospace and chemical engineering applications, and this particular alloy is the most used titanium alloy having a titanium market share of 60 % [16, 17].

Magnesium is the lightest structural metal and has attractive properties such as low density, high strength-to-weight ratio, good formability, and corrosion resistance. However, recently magnesium and its alloys have received an increased attention for use in automotive, aerospace, and electrical applications where weight reduction and specific strength are important factors for its choice [18, 19].

The ability to join Ti-6Al-4V to Mg-AZ31 can open up new avenues for product development especially in the aerospace industry. In this work, Ni coatings electrodeposited with a dispersion of nanoparticles of Ni, Cu, and

A. M. Atieh (✉) · T. I. Khan
Department of Mechanical and Manufacturing Engineering, University of Calgary, Calgary, AB T2N 1N4, Canada
e-mail: anas.m.attieh@gmail.com

T. I. Khan
Qatar Petroleum Chair, Department of Mechanical and Industrial Engineering, University of Qatar, Doha, Qatar

Ni/Cu were used as eutectic forming interlayers to join Mg-AZ31 alloy to the Ti-6Al-4V alloy. The effect of Ni and Cu nanoparticle dispersions on microstructural developments at the joint and subsequent effect on mechanical properties was investigated.

Experimental procedure

Base metal alloys of Ti-6Al-4V (6.7Al-4.4V-bal. Ti, wt%) and Mg-AZ31 (2.8Al-1.1Zn-bal. Mg, wt%) were used. Both alloys were received in the form of 10-mm-diameter rods. Samples 5 mm thick were cut and bonding surfaces were ground and polished to a 1000 grit finish. The Ti alloy surface was prepared for electrodeposition by soak cleaning the Ti-6Al-4V specimens with E-Kleen 102-E for 10 min, followed by a soak with E-Kleen 129-L for 2 min, and then acid pickling with 31 % HCl for 2 min. Before bonding, the Ti-6Al-4V was pickled for 3 min in 20 % HCl and 80 % distilled water, followed by acetone cleaning to remove surface oxides. The electrodeposition of Ni coatings was carried out in a 250-ml glass beaker using Watt's plating solution prepared by dissolving: 250 g $NiSO_4$ $6H_2O$, 45 g $NiCl_26H_2O$, 35 g H_3BO_3, 1 g Saccharin in 1 l of distilled water. Nanoparticles of Ni and Cu were introduced into the Ni bath at a concentration of 20 g/200 ml in three formats: Ni alone, Cu alone, and Ni/Cu together. The bath was ultrasonically agitated for 1 h, followed by magnetic stirring at 200 RPM for 1 h. Electrodeposition was carried out using a current density of 5 A/dm^2, with pH level maintained at 3.5, the coating temperature was kept at room temperature and the bath stirred at 200 RPM. The current density (5 A/dm^2) and deposition time (15 min) were used as a method of controlling coating thickness.

TLP bonding was carried out using R.F. induction heating in a vacuum chamber with a pressure of 4×10^{-4} Torr (0.053 Pa). The bonding temperature was set as 520 °C; bonding pressure as 0.2 MPa; and bonding time as 20 min. Joint characterisation was performed using scanning electron microscopy (SEM, JEOL JXA 8200) equipped with energy dispersive X-ray spectroscopy (EDS) for composition analysis. X-ray diffraction analysis was used to detect compounds formed at the fracture surface, A Rigaku Multiflex CuK_α radiation source with a step size 0.1° and step time 5 s is used at 40 kW and 20 mA over a scanning range 10°–90° two Theta (2Φ). To evaluate the mechanical properties of the joint, both microhardness measurements and shear strength tests were performed. A Vickers microhardness test was carried out using a Shimadzu mini-load microhardness tester with a 50 g load. Hardness profiles were established to a distance of 600 μm on each side of the load interface. The shear strength measurements were carried out using a 25 kN load-cell using a Tinius Olsen tensile test rig using a cross-head speed of 0.5 mm/min.

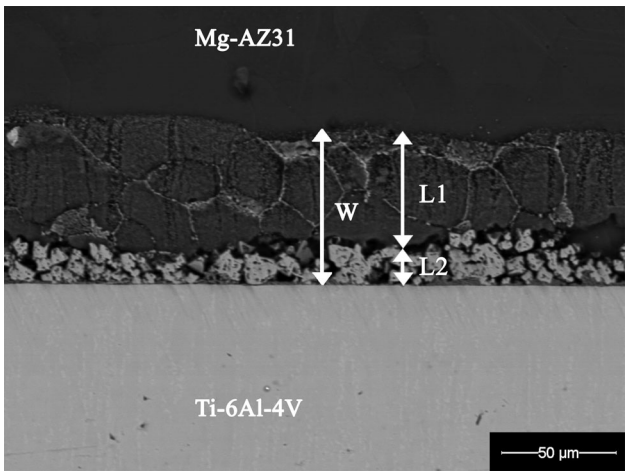

Fig. 1 SEM micrographs of Ti-6Al-4V/Ni nano/Mg-AZ31 joint interface after bonding at 520 °C and 0.2 MPa for 20 min

Results and discussion

Effect of nanoparticle dispersion on joint microstructure

The microstructure of a joint made at 520 °C, 0.2 MPa for 20 min using a coatings with a Ni nanoparticle dispersion is shown in Fig. 1. At the Mg-AZ31 bond interface, a grain boundary precipitate formed and EDS analysis revealed 60 % Mg, 37 % Al, 2 % Ni, and 1 % O. In comparison, the core of the grains showed a composition of 92 % Mg and 8 % Al. This observation showed that the diffusion of Al and Ni was greater along grain boundaries and this has been observed in the published literature [20]. Inside the joint region, the white "islands" showed a composition of 68 % Mg, 27 % Al, and 5 %Ni. The total width of the joint zone was measured to be about 58 μm. However, it was divided into two reaction layers, L1 and L2, where L1 was measured with a width of 41 μm and L2 with a width of 17 μm.

The SEM micrograph in Fig. 2 shows a joint interface for bonds made at 520 °C, 0.2 MPa for 20 min using a dispersion of Cu nanoparticles. The micrograph shows only one reaction layer with a total thickness of about 5 μm. This was attributed to the amount of liquid eutectic formed at the joint which was much less than that observed when bonding with a coating containing a Ni dispersion. The lower amount of eutectic formed could be due to the faster diffusion coefficients for Mg in Ni compared to Mg in Cu (The diffusion of Mg in Ni at 520 °C is 1.88×10^{-11} m^2 s^{-1} and the diffusion of Mg in Cu is 7.75×10^{-15} m^2 s^{-1} [20, 21]), resulting

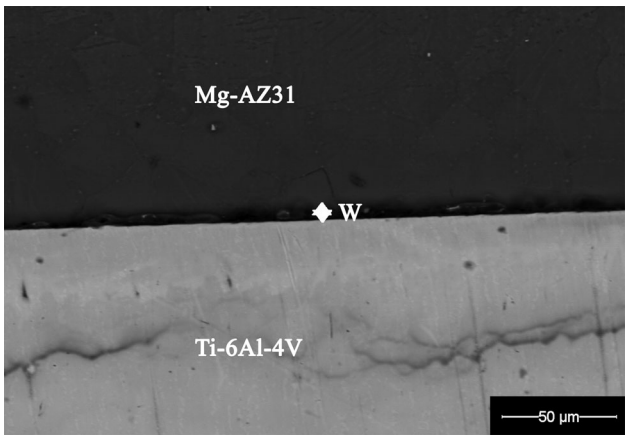

Fig. 2 SEM micrographs of Ti-6Al-4V/Cu nano/Mg-AZ31 joint interface after bonding at 520 °C and 0.2 MPa for 20 min

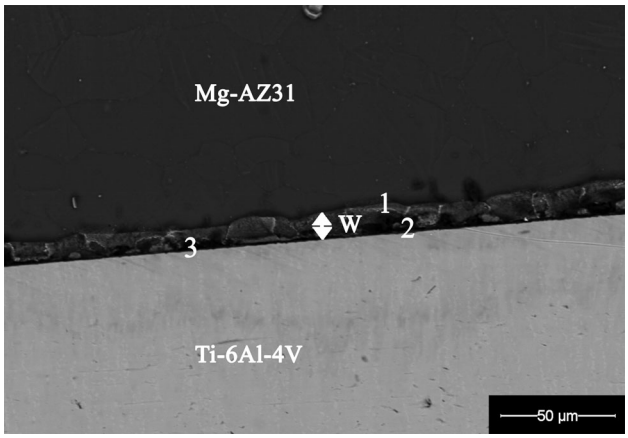

Fig. 3 SEM micrographs of Ti-6Al-4V/Cu-Ni nano matrix/Mg-AZ31 joint interface after bonding at 520 °C and 0.2 MPa for 20 min

in faster solidification at the joint. The elemental line analysis confirmed a low concentration of Cu and Ni (less than 1 at.%) inside the joint centerline. The EDS compositional analysis revealed that the reaction layer consisted of 69 % Mg, 16 % Al, 2 % O, 2 % Cu, and 1 % Ni.

The SEM micrograph in Fig. 3 shows a joint made at 520 °C, 0.2 MPa for 20 min using a coating containing a dispersion of Ni–Cu nanoparticles. Only one reaction layer of 15 μm thick formed at the joint. However, EDS analysis also showed that within the reaction layer the composition varied with different regions of the reaction layer. Table 1 shows the EDS analysis of the points as numbered in Fig. 3. The formation of different regions inside the reaction layer showed different chemical compositions. This suggested the formation of different intermetallic compounds which could be detrimental to the mechanical properties of the joint. Figure 4 shows the joint zone width as function of coating type.

Table 1 EDS point analysis (in wt%) taken from regions as shown in Fig. 3

Element	Mg	Al	Ti	Ni	Cu	O
1	92.4	7.0	0.0	0.2	0.0	0.3
2	74.2	13.7	5.6	4.4	0.0	2.0
3	63.8	21.9	9.9	0.8	1.8	1.7

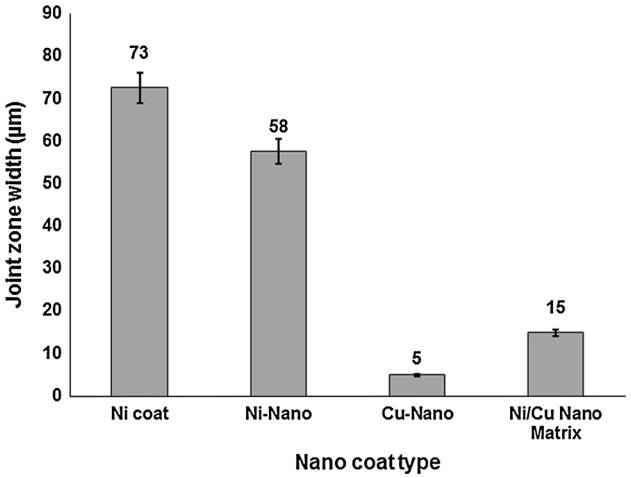

Fig. 4 Graph showing the effect of coat types on joint width

The literature suggests that nanoparticles have a high surface energy associated with them, and this can reduce the melting point of a bulk material [15, 22, 23]. Tiwari reported that the application of Ni nanoparticles for diffusion bonding of stainless steel 316 resulted in a 20 μm thick continuous reaction layer. In this work, the SEM micrograph in Figs 1, 2 and 3 shows that the Ni coating containing Ni and Cu nanoparticle dispersion reacted with the Mg-AZ31 alloy and melted to form the reaction layers. The literature suggests that the use of a multimetallic component alloy as an interlayer can enhance microstructural homogeneity and bond strength [24]. Tiwari and Paul [25] reported that nanopowder technology has received increased attention in many precision joining techniques such as integrated circuits and microsystem packaging. The Ni coating containing a dispersion of Ni and Cu nanoparticles was very thin and could accelerate the TLP bonding process because of the shorter diffusion distances.

The mechanism of joint formation occurred over three stages: solid-state diffusion and eutectic formation, dissolution of the Mg-AZ31 parent alloy followed by isothermal solidification of the joint. Solid-state diffusion of Ni in Mg and Ni in Ti and vise versa during the heating up stage to the bonding temperature is thought to occur before eutectic formation of Mg–Ni at the joint. It is thought that the formation of a metallurgical bond relies on two

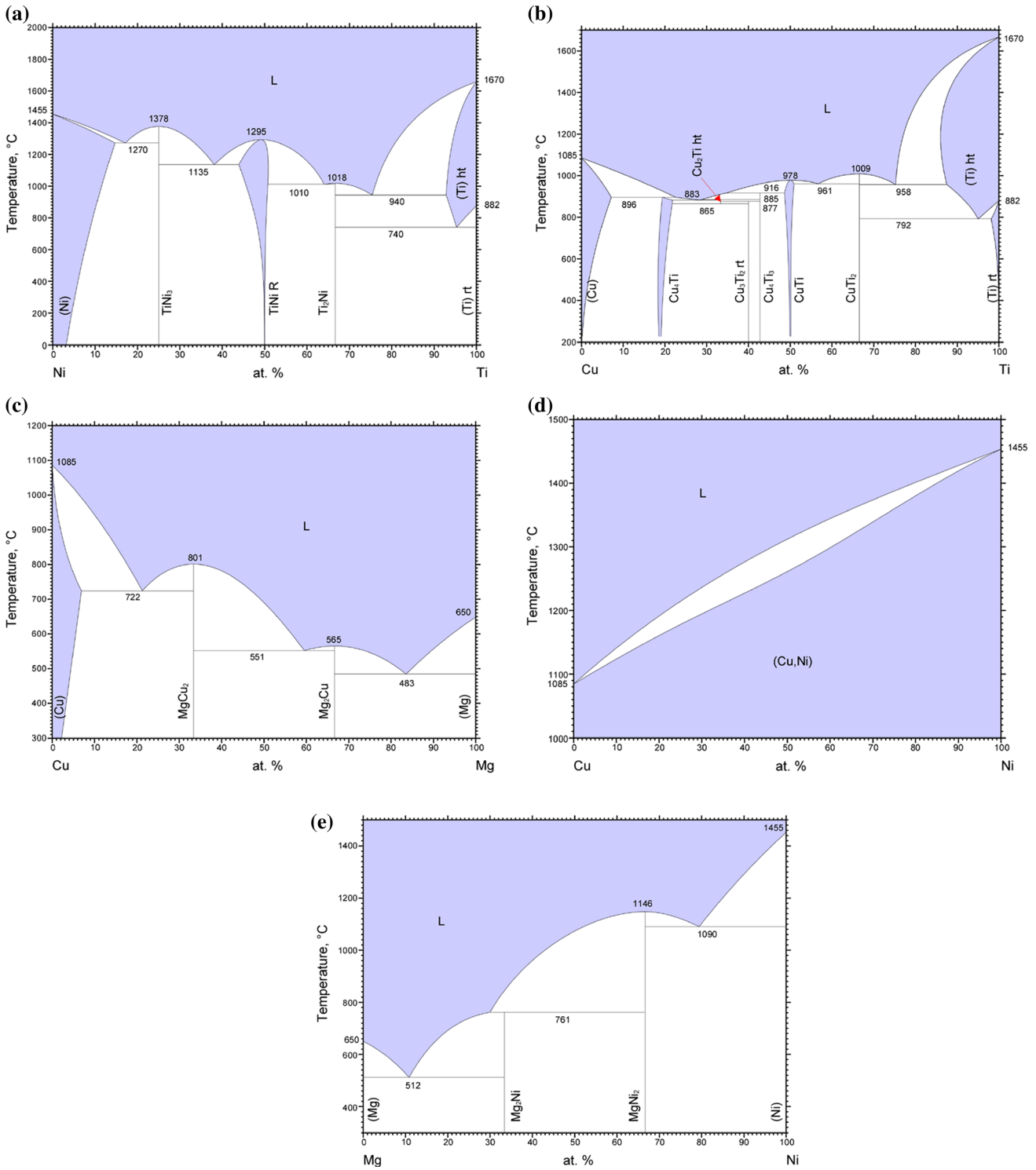

Fig. 5 Binary phase diagrams for **a** Ni–Ti [37] **b** Cu-Ti [38] **c** Cu-Mg [28] **d** Cu-Ni [39] **e** Mg-Ni [28]

mechanisms. First, solid-state diffusion at the Ti-6Al-4V alloy interface and second, solid-state diffusion followed by eutectic liquid formation at the Mg-AZ31 alloy interface. The phase diagrams in Figs. 5 and 6 for the Ti–Ni, Ti–Cu, and Ti–Ni–Cu systems suggest that no eutectic will form below a temperature of 883 °C. This temperature is higher than the bonding temperature of 520 °C.

As the Cu and Ni diffuse into the Mg, they form the intermetallic compounds illustrated in the phase diagram (e.g., $MgCu_2$). Because TLP bonding kinetics are controlled

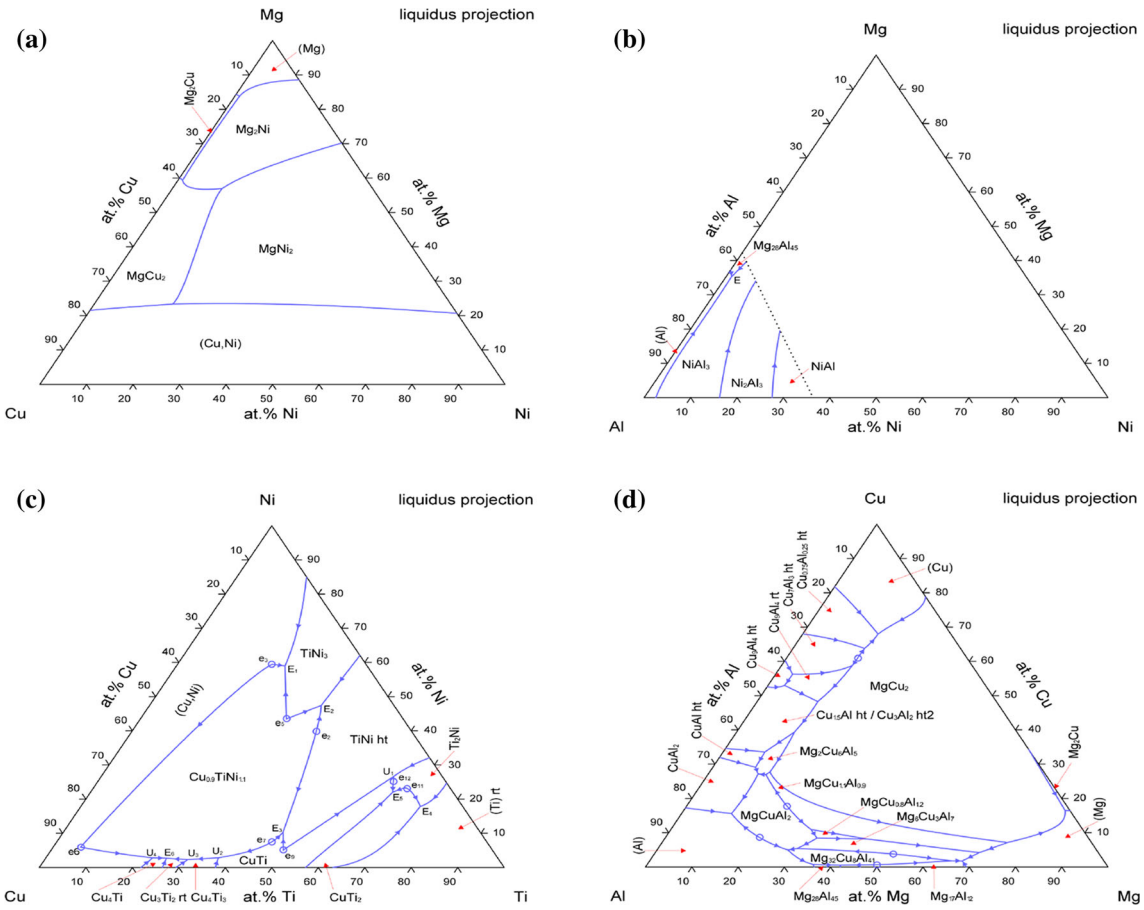

Fig. 6 Ternary phase diagrams for **a** Mg–Cu–Ni [28] **b** Mg–Al–Ni [40] **c** Ni–Cu–Ti [41] **d** Cu–Al–Mg [42]

by its isothermal nature, and due to the fairly high thermal conductivities of metals, the diffusion (horizontal sections of phase diagrams) will overrule the heating (vertical sections of phase diagrams), leading to melting occurring at controlled compositions (e.g., Mg and Mg_2Cu and the two liquidus lines between these compositions at 520 °C), as opposed to simply melting at the given composition of the eutectic temperature. These compositions surround the eutectic compositions that were mentioned for the Cu–Mg and Mg–Ni systems and are also important to bond kinetics.

According to the phase diagram for Ni–Cu (Fig. 5d), no eutectic is expected to form below a temperature of 1085 °C. The literature suggests that nanoparticles have high surface to volume ratio and it is thought that these particles will diffuse faster into the parent alloy than bulk foil material (i.e., foil interlayers) [15, 25]. This holds true for TLP bonding during the solid-state diffusion stage. Once the liquid state forms, it will have the same diffusion

Table 2 Theoretical determination of isothermal solidification times (t_{IS})

Dispersion type	Ni nanoparticle dispersion	Cu nanoparticle dispersion	Ni/Cu nanoparticle matrix dispersion
W^2_{max} (μm)	3364×10^{-12}	64×10^{-12}	225×10^{-12}
K^2	0.0169	0.0169	0.0169
D (m^2/S)	1.88×10^{-11}	1.88×10^{-11}	1.88×10^{-11}
t_{IS} (min)	11.03	0.21	0.74

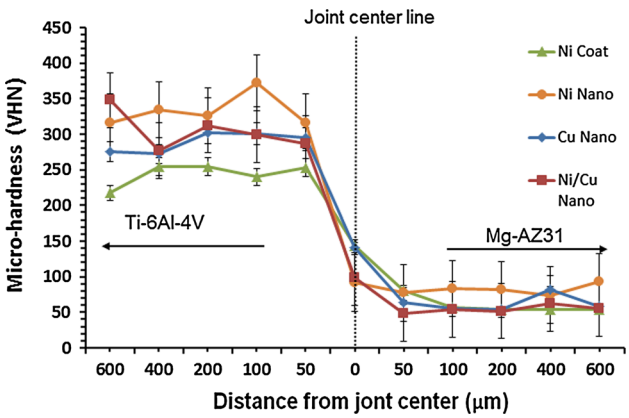

Fig. 7 Microhardness profile for joints made at 520 °C, 0.2 MPa for different coat types

rate as that of Mg–Ni and Mg–Cu liquid eutectic. In this work, the joint width was wider, when Ni nanoparticles were used as a dispersion than when Cu alone or Cu–Ni dispersions were used together, the wider joint (this observation) was expected to deteriorate the bond strength significantly [12, 26].

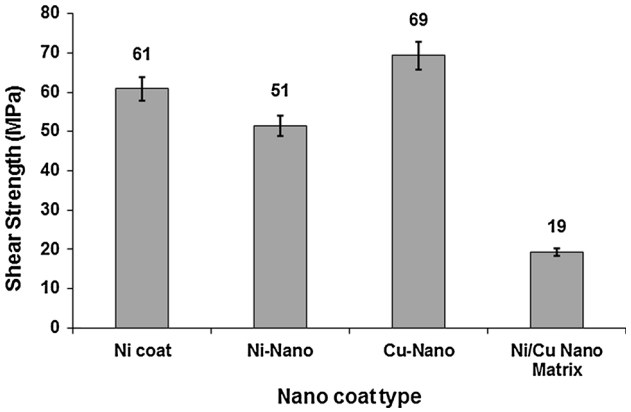

Fig. 8 Joint interface shear strength as a function of coat types for joints made at 520 °C, 0.2 MPa for 20 min

No ternary intermetallics are expected to form according to Fig. 6a in the Mg–Ni–Cu ternary system, and only binary intermetallics are possible [27, 28]. This observation was confirmed by this study, and no ternary Mg–Ni–Cu intermetallics were detected by the XRD analysis. The presence of Al in both alloys Mg-AZ31 alloy (2.7 wt% Al) and Ti-6Al-4V alloy (6.7 wt% Al) affected bond formation. For Mg–Ni–Al, the formation of $\tau = Ni_2Mg_3Al$ was expected. For Mg–Cu–Al, many intermetallics are expected to form (Fig. 6d), and the major intermetallic that expected to form is $Mg_2Cu_6Al_5$. Both Ni_2Mg_3Al and $Mg_2Cu_6Al_5$ were observed and detected by XRD analysis of the fracture surface in this research work. A comparison of joint widths for bonds made using a single Ni foil, double sandwich Ni-Cu foils, and Ni coatings showed that the thinnest reaction layers were obtained, when a dispersion of Ni and Cu nanoparticles was used [6, 7]. Thicknesses were 58, 5, and 15 μm for Ni-dispersed nanoparticles, Cu-dispersed nanoparticles and Ni–Cu dispersed nanoparticle matrix, respectively. The nanoparticles have high surface to volume ratio, and this encourages the formation of a eutectic faster and at a lower temperature than with a pure Ni coat or foil [29–31]. In this work, this observation of higher rate of diffusion of

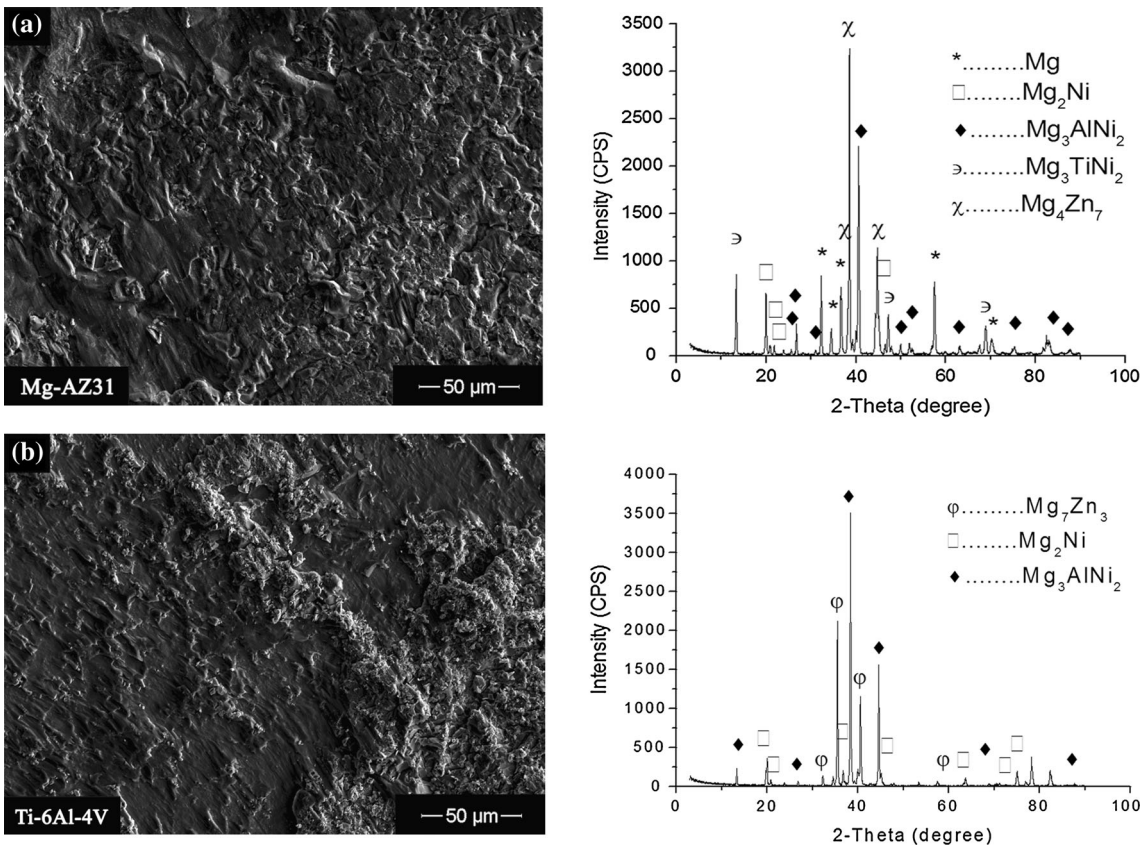

Fig. 9 SEM micrograph and XRD spectra of fractured surface for Ti-6Al-4V/Ni/Mg-AZ31 bond made at 520 °C, 0.2 MPa, and 20 min: **a** Mg-AZ31 side; **b** Ti-6Al-4V side

nanoparticles was observed in the microstructural developments across the joint region.

The microstructural developments of the joint showed that the time for isothermal solidification varied depending on the type of particle dispersion present in the coating. However, in the SEM micrograph, the formation of a lamellar structure in the eutectic phase and its disappearance indicated eutectic formation followed by completion of isothermal solidification. The time for isothermal solidification t_{IS} can be estimated by the equation [32]:

$$t_{IS} = \frac{W_{max}^2}{16K^2D} \quad (1)$$

Table 2 shows the estimated isothermal time for joint made using Ni and Cu nanoparticle dispersions. The minimum isothermal time t_{IS} corresponded to joints made with a Cu dispersion (0.21 min).

Microhardness measurements

The change in microhardness profiles across the joint interface for bonds made using the various nanoparticle dispersions is shown in Fig. 7. At a distance of 50–400 μm inside the Ti-6Al-4V alloy, the presence of Ni diffusion into the Ti alloy resulted in an increase in value to 372 VHN. This was attributed to the formation of a Ni–Ti solid-solution, and a similar observation was also observed at the Mg-AZ31 interface. The diffusion of Ni into the Mg alloy resulted in the formation of intermetallics at the Mg-AZ31 alloy interface and also an increase in hardness value to 93 VHN within the Mg alloy.

In comparison, the hardness values for joints made with Cu or Cu–Ni nano dispersions resulted in lower microhardness profiles. At a distance of 100–200 μm inside the Mg-AZ31 alloy, a similar hardness profile of 65 VHN was recorded and was not affected by the type of dispersion used at the joint.

The compositional homogeneity of the joint can be assessed by microhardness testing across the joint region. In general, a uniform hardness across the joint interface indicates a good homogeneity. The results in Fig. 7 indicate a uniformity in microhardness on either side of the joint region suggesting that solid-solution strengthening is attained by the interdiffusion of elements across the joint

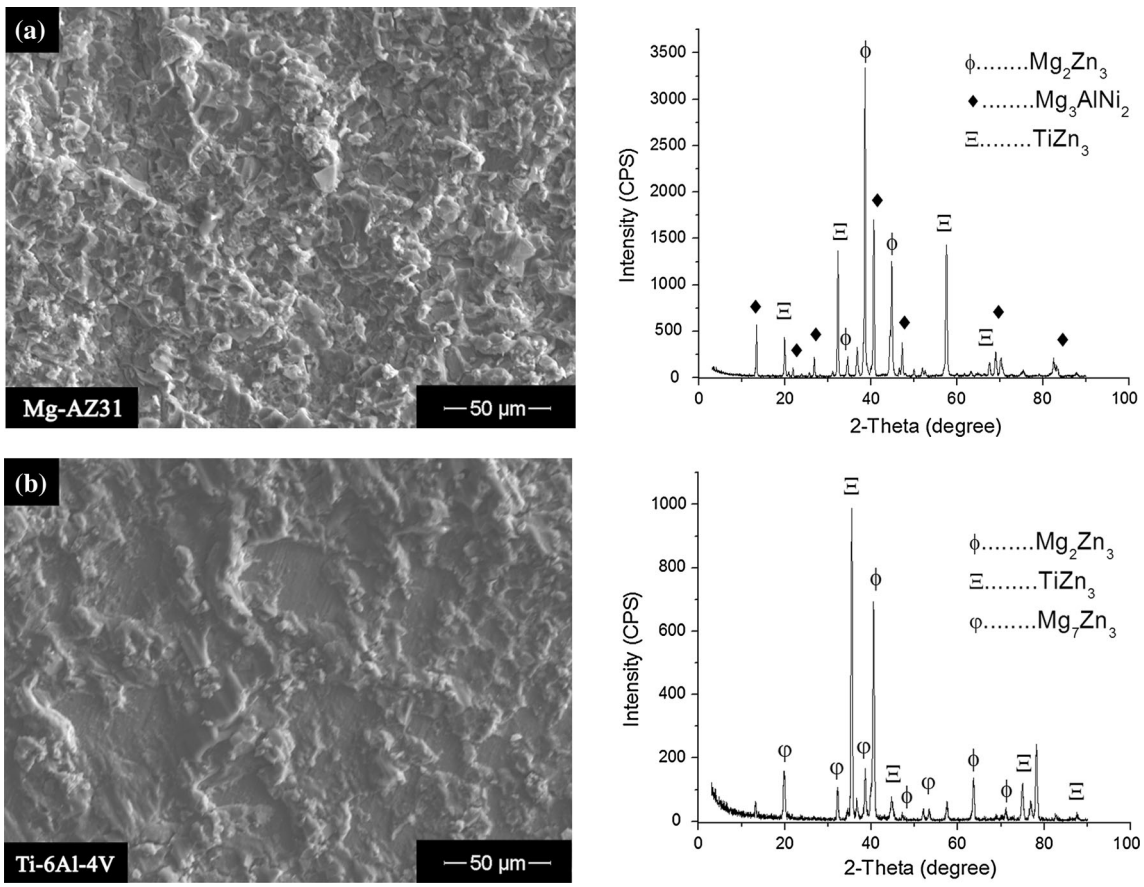

Fig. 10 SEM micrograph and XRD spectra of fractured surface for Ti-6Al-4V/Ni nano/Mg-AZ31 bond made at 520 °C, 0.2 MPa, and 20 min: **a** Mg-AZ31 side; **b** Ti-6Al-4V side

region. Furthermore, the presence of a dispersion of nanoparticles within the joint gives a higher hardness profile compared to joints made with Ni coating without dispersion. This observation was particularly noticeable at the Ti-6Al-4V joint interface. In addition to solid-solution strengthening, the presence of fine intermetallics dispersed within the joint can also increase the hardness values across the joint region. Furthermore, it is suggested that the nanoparticles cause a higher strain-hardening rate and this resulted in an increase the hardness [13, 33].

Shear strength evaluation

The joint shear strength values obtained for bonds made at 520 °C, 0.2 MPa for 20 min can be seen in Fig. 8. Joints made with a dispersion of Ni nanoparticles gave shear strength value of 51 MPa which was lower than the 61 MPa value achieved when using pure Ni coatings. It is thought that less Ni–Mg eutectic liquid formed when bonding with Ni dispersion due to the higher diffusivity of Ni nanoparticles toward the Ti alloy interface.

Joints made with a dispersion of Cu nanoparticles gave a maximum shear strength value of 69 MPa. This value was double the value reported for bonds made using Ni foils (36 MPa). This value was also higher than the shear strength values obtained when adhesive bonding or spot welding was used to join these alloys [5, 34, 35].

However, when a Ni coating with Ni/Cu nanoparticle dispersion was used to form a joint, a decrease in joint shear strength was observed to 19 MPa. This drop in shear strength was attributed to the segregation of Mg–Ni, Mg–Cu, and Ni–Cu intermetallics within the joint center forming inhomogeneous single reaction layer.

Tiwari and Paul [15, 25] reported that a dispersion of Ni nanoparticles produced a joint with a higher shear strength at lower bonding temperature than joints made without nanoparticles. Furthermore, the bond interface has less brittle intermetallics and phases as well as less voids. However, in this research work, it is shown that the type of nanoparticles influences joint strengths. The use of Cu nanoparticles dispersion gave the best joint shear strength values of 69 MPa.

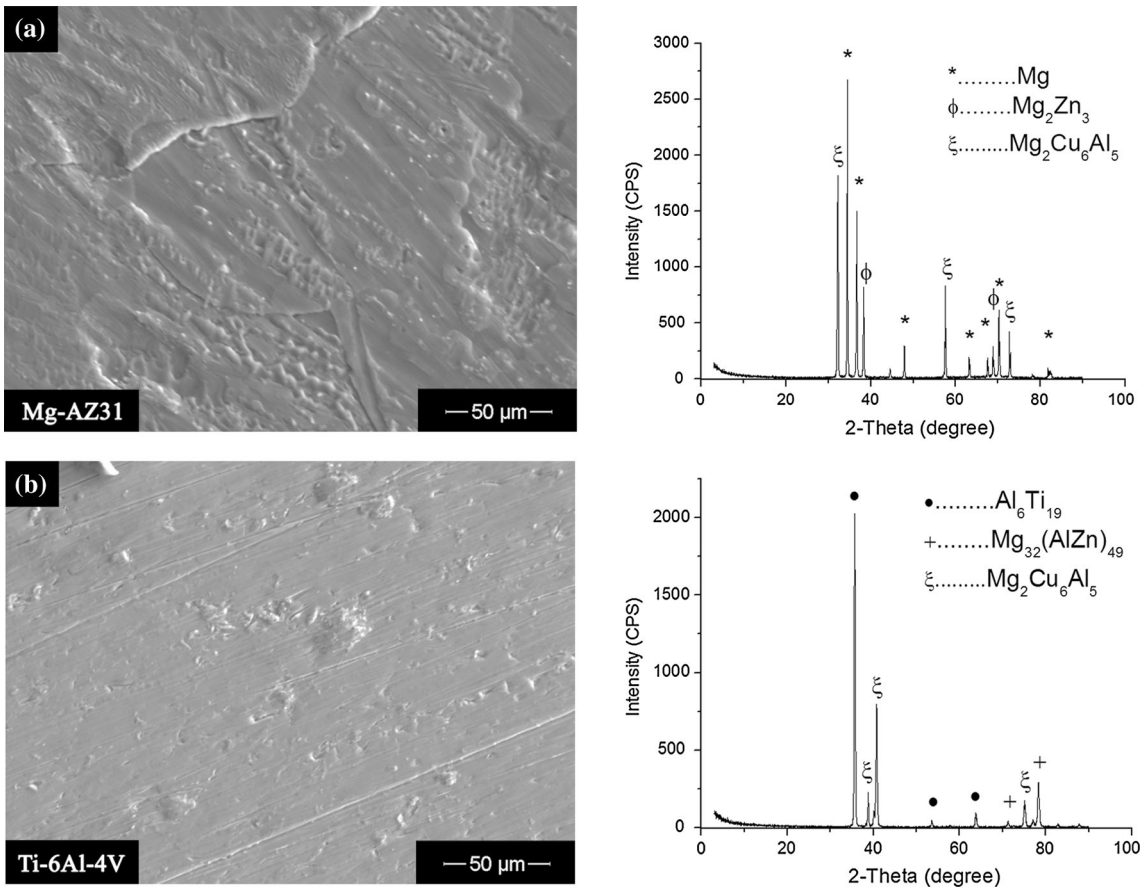

Fig. 11 SEM micrograph and XRD spectra of fractured surface for Ti-6Al-4V/Cu nano/Mg-AZ31 bond made at 520 °C, 0.2 MPa, and 20 min: **a** Mg-AZ31 side; **b** Ti-6Al-4V side

Fractography and XRD analysis

The SEM micrograph and XRD spectra obtained from Mg-AZ31 and Ti-6Al-4V alloys fractured surface are shown in Figs. 9, 10, 11 and 12. When Ni coats without a dispersion were used, both fracture surfaces showed a mixed ductile/brittle failure mode. Two intermetallic phases were commonly detected at the fracture surfaces of both alloys, the eutectic phase Mg_2Ni and the ternary phase Mg_3AlNi_2. Furthermore, no Ti–rich phase or intermetallics were detected at the fracture surface of the Ti-6Al-4V alloy. This observation suggested that the fracture propagated through the center of the joint and close to the Mg-AZ31 interface.

Joints made using a Ni nanoparticle dispersion produced a ductile failure mode (Fig. 10). Furthermore, Mg_2Zn_3 and $TiZn_3$ peaks were detected on both the Mg-AZ31 and Ti-6Al-4V alloy fracture surfaces. This suggested that the direction of crack propagation deviated from one joint interface to the other.

Joints made with a dispersion of Cu nanoparticles gave a failure mode that was brittle (Fig. 11). The SEM micrograph in Fig. 2 showed that the width of the joint zone was less than 10 μm, and this suggested that the fracture propagated in this joint zone. This observation was confirmed by the detection of Mg and Mg_2Zn_3 at the Mg-AZ31 fracture surface, and Al_6Ti_{19} at Ti-6Al-4V fracture surface. Furthermore, a ternary phase of $Mg_2Cu_6Al_5$ was detected, and this was anticipated because the Cu–Mg eutectic temperature (485 °C) [27] was less than the Ni–Mg eutectic temperature (508 °C) [36]. Once these compounds formed inside the joint region, these compounds remained within the joint zone.

Joints made using a dispersion of Ni/Cu nanoparticles produced Cu–Mg eutectic phase ($CuMg_2$) at the joint (Fig. 12). Furthermore, no Ti-rich phase was detected at the Ti-6Al-4V fracture surface indicating that the fracture path propagated away from Ti-6Al-4V alloy interface and close to the Mg-AZ31 interface.

Conclusion

The TLP bonding of Mg-AZ31 to a Ti-6Al-4V alloy using a dispersion of Ni and Cu nanoparticles was successful in

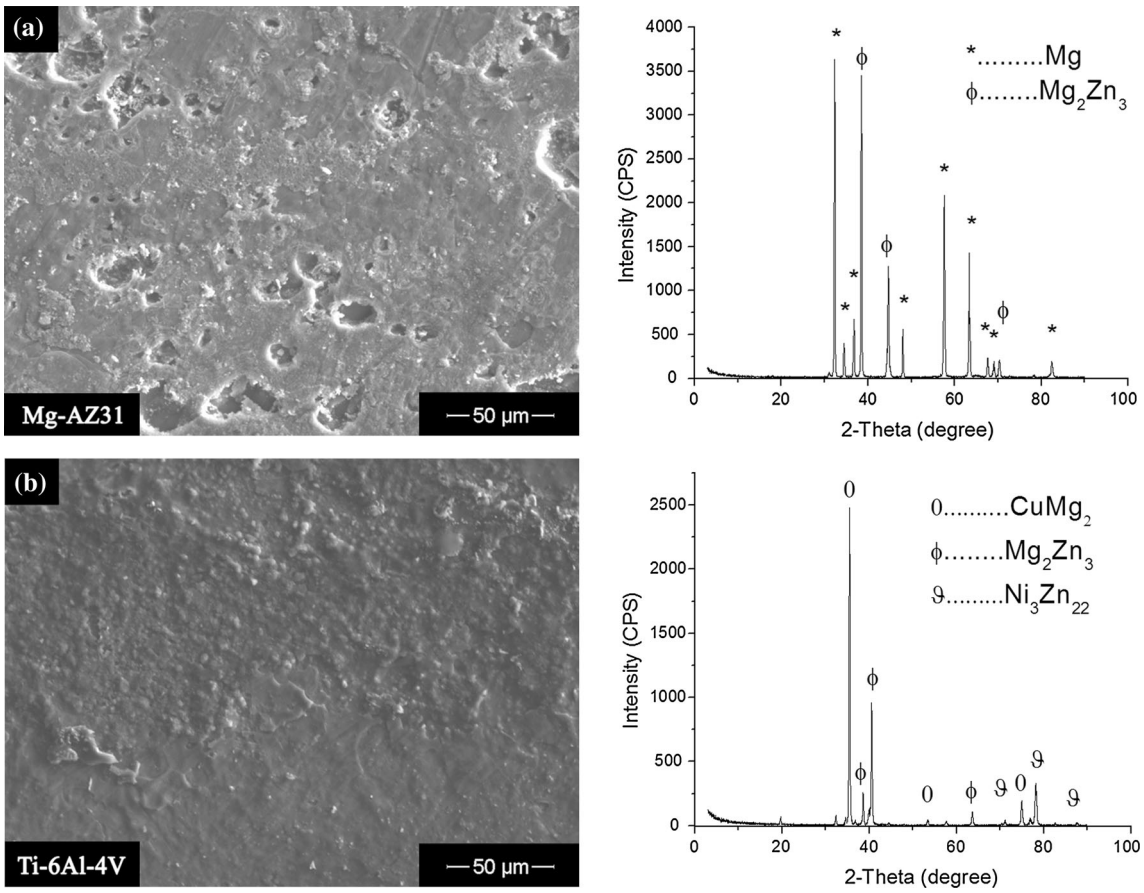

Fig. 12 SEM micrograph and XRD spectra of fractured surface for Ti-6Al-4V/Ni-Cu nano matrix/Mg-AZ31 bond made at 520 °C, 0.2 MPa, and 20 min: **a** Mg-AZ31 side; **b** Ti-6Al-4V side

achieving joints. This work showed that the presence of nanoparticles within the joint region enhances joint formation by affecting the isothermal solidification rate during the bonding process. The type of dispersion (i.e. Ni, Cu, or Ni and Cu) affects the thickness of liquid eutectic formed at the joint and this influences the type of intermetallics formed at the joint. The use of a Ni dispersion produced intermetallics of Mg_2Ni and Mg_3AlNi_2 and these changed to $CuMg_2$ and $Mg_2Cu_6Al_5$ when a Cu dispersion was used within the coating. A maximum joint shear strength of 69 MPa was achieved when a Cu nanoparticle dispersion was used.

Acknowledgements The authors would like to acknowledge The German Jordanian University (GJU), and NSERC Canada for the financial support for this research.

References

1. Sakiyama T, Murayama G, Kenji S et al (2013) Dissimilar metal joining technologies for steel sheet and aluminum alloy sheet in auto body. Nippon Steel Tech Rep 103:91–98
2. AlHazaa A, Khan TI, Haq I (2010) Transient liquid phase (TLP) bonding of Al7075 to Ti–6Al–4V alloy. Mater Charact 61:312–317
3. Elthalabawy W, Khan TI (2011) Liquid phase bonding of 316L stainless steel to AZ31 magnesium alloy. J Mater Sci Technol 27:22–28
4. Chang C-T, Shiue R-K (2006) Infrared brazing of Ti-6Al-4V using the Ti-15Cu-15Ni braze alloy. J Mater Sci 41:2145–2150. doi:10.1007/s10853-006-5242-7
5. Jin YJ, Khan TI (2012) Effect of bonding time on microstructure and mechanical properties of transient liquid phase bonded magnesium AZ31 alloy. Mater Des 38:32–37. doi:10.1016/j.matdes.2012.01.039
6. Atieh AM, Khan TI (2013) Effect of process parameters on semi-solid TLP bonding of Ti–6Al–4V to Mg–AZ31. J Mater Sci 48:6737–6745. doi:10.1007/s10853-013-7475-6
7. Atieh AM, Khan TI (2014) Transient liquid phase (TLP) brazing of Mg-AZ31 and Ti-6Al-4V using Ni and Cu sandwich foils. Sci Technol Weld Join. doi:10.1179/1362171814Y.0000000196
8. Sun D, Gu X, Liu W (2005) Transient liquid phase bonding of magnesium alloy (Mg-3Al-1Zn) using aluminum interlayer. Mater Sci Eng A 391:29–33
9. Saha RK, Khan TI (2009) Microstructural developments in TLP bonds using thin interlayers based on Ni–B coatings. Mater Charact 60:1001–1007. doi:10.1016/j.matchar.2009.04.002
10. Cook G, Sorensen C (2011) Overview of transient liquid phase and partial transient liquid phase bonding. J Mater Sci 46:5305–5323. doi:10.1007/s10853-011-5561-1
11. Zhou Y, Gale WF, North TH (1995) Modelling of transient liquid phase bonding. Int Mater Rev 40:181–196. doi:10.1179/095066095790151160
12. Zhang G, Zhang J, Pei Y et al (2008) Joining of Al_2O_3p/Al composites by transient liquid phase (TLP) bonding and a novel process of active-transient liquid phase (A-TLP) bonding. Mater Sci Eng A 488:146–156. doi:10.1016/j.msea.2007.11.084
13. Cooke KO (2012) A study of the effect of nanosized particles on transient liquid phase diffusion bonding Al6061 metal-matrix composite (MMC) Using Ni/Al_2O_3 nanocomposite interlayer. Metall Mater Trans B 43:627–634. doi:10.1007/s11663-012-9643-5
14. Cooke KO, Khan TI, Oliver GD (2012) Transient liquid phase diffusion bonding Al-6061 using nano-dispersed Ni coatings. Mater Des 33:469–475. doi:10.1016/j.matdes.2011.04.051
15. Tiwari SK (2010) Nickel Nanoparticles-Assisted Diffusion Brazing of Stainless Steel 316 for Microfluidic Applications. Oregon State University
16. Smith WF (1993) Structure and properties of engineering alloys. McGraw-Hill Inc, New York
17. Chang CT, Shiue RK (2005) Infrared brazing Ti–6Al–4V and Mo using the Ti–15Cu–15Ni braze alloy. Int J Refract Met Hard Mater 23:161–170. doi:10.1016/j.ijrmhm.2005.01.002
18. Kulekci MK (2007) Magnesium and its alloys applications in automotive industry. Int J Adv Manuf Technol 39:851–865. doi:10.1007/s00170-007-1279-2
19. Friedrich HE, Mordike BL (2006) Magnesium Technology Metallurgy, Design Data, and Applications. doi: 10.1007/3-540-30812-1
20. Elthalabawy W (2010) Diffusion Bonding behavior and characterization of joints made between 316L stainless steel alloy and AZ31 magnesium alloy. University of Calgary
21. Vušanovi I, Voronjec D, Krane MJM (2001) Microsegregation phenomena in Al–Cu–Mg alloy with considering of diffusion phenomena in primary phase. Facta Univ 1:965–980
22. Castro T, Reifenberger R, Choi E, Andres RP (1990) Size dependence melting point of individual nanometer-sized metallic clusters. Phys Rev B 42:8548–8557
23. Jiang H, Moon K, Dong H et al (2006) Size-dependent melting properties of tin nanoparticles. Chem Phys Lett 429:492–496
24. Ryan EJ (1988) Titanium–copper–nickel braze filler metal and method of brazing. US Patent US4725509A, 18 Feb 1986
25. Tiwari SK, Paul BK (2010) Comparison of nickel nanoparticle-assisted diffusion brazing of stainless steel 316 to conventional diffusion brazing and bonding processes. J Manuf Sci Eng 132(3):030902-1–030902–5
26. Sayyedain SS, Salimijazi HR, Toroghinejad MR, Karimzadeh F (2014) Microstructure and mechanical properties of transient liquid phase bonding of / Al nanocomposite using copper interlayer. Mater Des 53:275–282. doi:10.1016/j.matdes.2013.06.074
27. Gupta KP (2004) The Cu–Mg–Ni (Copper–Magnesium–Nickel) System. J Phase Equilibria Diffus 25:471–478. doi:10.1361/15477030420214
28. Miettinen J (2008) Thermodynamic description of Cu–Mg–Ni and Cu–Mg–Zn systems. CALPHAD Comput Coupling Phase Diagrams Thermochem / ASM Alloy Phase Diagrams Center 32:389–398
29. Lee J, Mori H, Tanaka T, Penttilä K (2005) Phase diagrams of nanometer-sized particles in binary systems. JOM 57:56–59. doi:10.1007/s11837-005-0235-6
30. Lee J-G, Mori H, Yasuda H (2005) In situ high-resolution electron microscope observation of phase change in nanometer-sized alloy particles. J Mater Res 20:1708–1721. doi:10.1557/JMR.2005.0223
31. Schamp C, Jesser W (2006) Two-phase equilibrium in individual nanoparticles of Bi–Sn. Metall Mater Trans A 37:1825–1829
32. Tuah-Poku I, Dollar M, Massalski T (1988) A study of the transient liquid phase bonding process applied to a Ag/Cu/Ag sandwich joint. Metall Trans A 19:675–686
33. Tjong SC (2007) Novel nanoparticle-reinforced metal matrix composites with enhanced mechanical properties. Adv Eng Mater 9:639–652. doi:10.1002/adem.200700106
34. Sun DQ, Lang B, Sun DX, Li JB (2007) Microstructure and mechanical properties of resistance spot welded magnesium alloy joints. Mater Sci Eng A 460–461:494–498
35. Tang Y, Zhao X, Jiang K et al (2010) The influences of duty cycle on the bonding strength of AZ31B magnesium alloy by

microarc oxidation treatment. Surf Coat Technol 205: 1789–1792
36. Okamoto H (2007) Mg–Ni (Magnesium–Nickel) supplemental literature review: section III. J Phase Equilibria Diffus 28:303. doi:10.1007/s11669-007-9058-1
37. Bormann R, Zöltzer K (1992) Determination of the thermodynamic functions and calculation of phase diagrams for metastable phases. Phys Status Solidi A / ASM Alloy Phase Diagrams Center 131:691–705
38. Turchanin MA, Agraval PG, Abdulov AR (2008) Thermodynamic assessment of the Cu–Ti–Zr system. I. Cu–Ti system. Powder Metall Met Ceram / ASM Alloy Phase Diagrams Center 47:344–360
39. Miettinen J (2005) Thermodynamic description of the Cu–Al–Ni system at the Cu–Ni side, Cu–Ni phase diagram. CALPHAD Comput Coupling Phase Diagrams Thermochem / ASM Alloy Phase Diagrams Center 29:40–48
40. Prima SB (1993) Aluminium–magnesium–nickel, ternary alloys. VCH/ASM Alloy Phase Diagrams Cent 6:454–459
41. Gupta KP (2002) The Cu–Ni–Ti (copper–nickel–titanium) system. J Phase Equilibria / ASM Alloy Phase Diagrams Center 23:541–547
42. Buhler T, Fries SG, Spencer PJ, Lukas HL (1998) A thermodynamic assessment of the Al–Cu–Mg ternary system. J Phase Equilibria / ASM Alloy Phase Diagrams Center 19:317–333